

# The effect of the neutron and proton numbers ratio in colliding nuclei at formation of the evaporation residues in the $^{34}\text{S}+^{208}\text{Pb}$ and $^{36}\text{S}+^{206}\text{Pb}$ reactions.

A.K. Nasirov<sup>1,2</sup>, B.M. Kayumov<sup>2</sup>, G. Mandaglio<sup>3,4</sup>, G. Giardina<sup>5</sup>, K. Kim<sup>6</sup>, Y. Kim<sup>6</sup>

<sup>1</sup> BLTP, Joint Institute for Nuclear Research, Joliot-Curie 6, 141980 Dubna, Russia

<sup>2</sup> Institute of Nuclear Physics, Ulugbek, 100214, Tashkent, Uzbekistan

<sup>3</sup> Dipartimento di Scienze Chimiche, Biologiche, Farmaceutiche ed Ambientali, University of Messina, Messina, Italy

<sup>4</sup> INFN Sezione di Catania, Catania, Italy

<sup>5</sup> Dipartimento di Scienze Matematiche e Informatiche, Scienze Fisiche e Scienze della Terra, University of Messina, Messina, Italy

<sup>6</sup> Rare Isotope Science Project, Institute for Basic Science, Daejeon 305-811, Republic of Korea

Received: date / Revised version: date

**Abstract.** The difference between observed cross sections of the evaporation residues (ER) of the  $^{34}\text{S}+^{208}\text{Pb}$  and  $^{36}\text{S}+^{206}\text{Pb}$  reactions formed in the 2n and 3n channels has been explained by two reasons related with the entrance channel characteristics of these reactions. The first reason is that the capture cross section of the latter reaction is larger than the one of the  $^{34}\text{S}+^{208}\text{Pb}$  reaction since the nucleus-nucleus potential is more attractive in the  $^{36}\text{S}+^{206}\text{Pb}$  reaction due to two more neutrons in isotope  $^{36}\text{S}$ . The second reason is the difference in the heights of the intrinsic fusion barrier  $B_{\text{fus}}^*$  appearing on the fusion trajectory by nucleon transfer between nuclei of the DNS formed after the capture. The value of  $B_{\text{fus}}^*$  calculated for the  $^{34}\text{S}+^{208}\text{Pb}$  reaction is higher than the one obtained for the  $^{36}\text{S}+^{206}\text{Pb}$  reaction. This fact has been caused by the difference between the  $N/Z$ -ratios in the light fragments of the DNS formed during the capture in these reactions. The  $N/Z$ -ratio has been found by solution of the transport master equations for the proton and neutron distributions between fragments of the DNS formed at capture with the different initial neutron numbers  $N = 18$  and  $N = 20$  for the reactions with the  $^{34}\text{S}$  and  $^{36}\text{S}$ , respectively.

**Key words.** capture, potential energy, complete fusion, evaporation residues

**PACS.** 25.70.Hi Transfer reactions – 25.70.Jj Fusion and fusion-fission reactions

## 1 Introduction

The complete fusion of two colliding nuclei and de-excitation of the formed excited compound nucleus (CN) are topics of a great interest in physics of nuclear reaction. The de-excitation of the CN through the evaporation of neutrons can lead to the synthesis of the heaviest elements (with the charge numbers  $Z = 108-118$ ). A significant difficulty in producing the heaviest elements in fusion-evaporation reactions is very small cross sections, which can be attributed to the hindrance at the formation of the CN and/or to its instability against fission. The high accuracy of measurements of the ER cross section stimulates studies of the peculiarities of the reaction mechanism in experiments producing transuranic elements. For this aim, in Ref.[1], the authors compared two reactions with the different isotopes of S and Pb leading to the same nucleus  $^{242}\text{Cf}$ . The measured cross section for the 2n channel of  $^{36}\text{S}+^{206}\text{Pb}$  was approximately 25 times larger than that of  $^{34}\text{S}+^{208}\text{Pb}$ . In the case of the 3n channel, approximately ten times larger cross section was measured for the  $^{36}\text{S}+^{206}\text{Pb}$  reaction compared to the  $^{34}\text{S}+^{208}\text{Pb}$  reaction. These values were obtained close to the maxima of the 2n and 3n cross sections. In Ref.[2], the experimental data of the yield of fission products have been obtained to establish the main reasons causing the difference in the results of the evaporation residue cross sections in the above mentioned reactions. The excitation function of

fission for the  $^{36}\text{S}+^{206}\text{Pb}$  reaction is higher than the one of the  $^{34}\text{S}+^{208}\text{Pb}$  reaction if they are compared as functions of the CN excitation energy. In Ref. [1], the authors noted that the difference of only two neutrons in projectile and target nuclei has such a strong influence on the fusion probability. This amazing result requests its further explanation.

The first attempt was made by the authors of the experiments in Ref.[1] by the description of the fission excitation functions using the coupled-channels calculations (code CCFULL [3]) with coupling to vibrational states; the evaporation residue cross sections were estimated by the statistical code HIVAP [4], normalizing the capture cross section calculated by the HIVAP to the measured capture cross sections. Regardless of this procedure, the authors modified the parameters of the HIVAP code for the survival probability of  $^{242}\text{Cf}^*$  such that the measured ER cross sections of the  $^{36}\text{S}+^{206}\text{Pb}$  reaction were reproduced at  $E^* = 25.5$  and  $33.1$  MeV for the 2n and 3n channels, respectively. This action allowed authors to reproduce the ER cross sections of the  $^{36}\text{S}+^{206}\text{Pb}$  reaction, but at the use of the same parameters leads to overestimation of the measured data of the  $^{34}\text{S}+^{208}\text{Pb}$  reaction. Therefore, authors have concluded that the latter reaction exhibits a significant hindrance of fusion relative to the  $^{36}\text{S}+^{206}\text{Pb}$  reaction. Another attempt to clarify the nature of the hindrance to complete fusion in the case of the  $^{34}\text{S}+^{208}\text{Pb}$  reaction has been done in Ref.[2]. The authors of Ref.[2] have used new fission measurements and existing evaporation residue and fission excitation function data

---

*Send offprint requests to:* Avazbek Nasirov

*Correspondence to:* Joint Institute for Nuclear Research,  
Joliot-Curie 6, 141980 Dubna, Russia

for reactions forming Cf isotopes to investigate the dependence of the quasifission probability and characteristics of fission products on the properties of the entrance channels. The calculations made by the use of the coupled-channels code CCFULL reproduce the measured capture cross sections for both reactions. Assuming no quasifission ( $P_{CN}=1$ ), the statistical model calculations of the fission survival probability  $W_{CN}$  are able to reproduce the measured xn ER cross sections for the  $^{36}\text{S}+^{206}\text{Pb}$  reaction. However, the calculations made by the use of the same parameters have led to the overestimation of the experimental xn ER cross sections for the  $^{34}\text{S}+^{208}\text{Pb}$  reaction. The agreement with the experimental data of the last reaction can be reached by introducing a strong fusion hindrance for it relative to the  $^{36}\text{S}+^{206}\text{Pb}$  reaction (with an angular momentum averaged hindrance  $P_{CN}=0.1$ ). This procedure must be associated with a large quasifission probability for  $^{34}\text{S}+^{208}\text{Pb}$ . The analysis of mass and angle distributions of the fusion-fission products of these two reactions did not reveal a significant difference between them showing the hindrance in fusion. The authors concluded that the strongly hindered ER yield for the  $^{34}\text{S}+^{208}\text{Pb}$  reaction compared with the  $^{36}\text{S}+^{206}\text{Pb}$  reaction indicates that the quasifission competition is weaker in the  $^{36}\text{S}+^{206}\text{Pb}$  reaction. This must be attributed to the different nuclear structures of the reaction partners in the two reactions and closer matching of N/Z ratios in the latter reaction, as found in Ca + Pb reactions [5]. The authors could not explain the appearance of the hindrance to fusion causing the value  $P_{CN}=0.1$ . One of the reasons of difficulties in

study of hindrance to fusion is difference in the theoretical and experimental views to the capture events.

In this work we try to establish reasons causing difference at the CN formation in the two reactions under discussions by the theoretical analysis of the formation of dinuclear system (DNS) after capture and its transformation into the CN. In Section 2 the different views in estimation of the capture cross section are shortly discussed. The methods of calculations are briefly presented in Section 3 and results of the capture and fusion cross sections are discussed in Section 4.

## 2 Different views to the definition of capture

In the deep-inelastic collisions, the full momentum transfer of the relative motion does not take place and interaction time of the colliding nuclei is relatively shorter than in the case of capture reactions which request the full momentum transfer. The main difference between deep-inelastic collision and capture events, which can be observed in experiment, is a value of the total kinetic energy of the reaction products. The total kinetic energy of the products formed in the capture reaction are fully damped and its value is significantly lower than the initial collision energy  $E_{c.m.}$ , while the total kinetic energy of the deep-inelastic collisions products is not fully damped and its value is close to the  $E_{c.m.}$ . The DNS formed as a result of the capture of the colliding nuclei can evolve to one of states of the heated and rotating compound nucleus (complete fusion) or it breaks down forming two fragments (quasifission) without reaching the saddle point of CN.

The mass and charge distributions of the deep-inelastic collision and capture events can widely overlap. This overlaps of the mass and charge distributions have been discussed in Ref. [6] for the case of  $^{48}\text{Ca}+^{208}\text{Pb}$  reaction. The main conclusion from this short comment is that capture events are presented as the yield of the projectile- and target-like products with the total kinetic energy significantly lower than the initial collision energies. The total kinetic energy of the products formed in the capture reaction are around their Coulomb barriers in the exit channels since the amount of the kinetic energy of the relative motion above the Coulomb barrier is dissipated, *i.e.* the full momentum of the relative motion occurs. The difference between the total kinetic energies of the products formed in the deep-inelastic collision and capture events depends on the projectile-nucleus energy, orbital angular momentum of collision, mass and charge numbers of the colliding nuclei. Unfortunately, there is not so many experimental and theoretical studies devoted to the important problem which allows us to draw interesting conclusions about reaction mechanism of the heavy-ion collisions at the energies near the Coulomb barrier. Since the events producing projectile-like and target-like binary products are considered as the deep-inelastic collision events only. Therefore, the separation of the capture events producing projectile-like and target-like binary products from the deep-inelastic collision events requests detailed analysis of the experimental data and developing corresponded theoretical methods. Nevertheless, there are papers where the authors have studied the properties of the reaction prod-

ucts by the analysis of their total kinetic energies. For example, in Fig. 3 of Ref.[7], the yield of the binary products with the mass numbers in the range  $M_1 = 40-56$  of the  $^{50}\text{Cr}+^{208}\text{Pb}$  reaction and having total kinetic energy around 235 MeV are shown as to be belonged to quasilastic and the ones having the total kinetic energy around 160 MeV are marked as the products of the deep-inelastic collisions. All of the products with the mass numbers in the range  $M_1 = 57-82$  are indicated as ones of the fast quasifission process. According to our point of view, among the products marked the deep-inelastic collisions there are events of the quasifission having the total kinetic energy approximately in the range 150-170 MeV. More detailed analysis should be performed in our future research devoted to this topic. The yield of the projectile- and target-like products of the capture reactions is responsible for the decrease of the events going to the complete fusion and this mechanism can be considered as hindrance to complete fusion which is not studied by experimentalists.

The correct estimated quasifission cross section  $\sigma_{\text{qf}}$  contains a contribution of the yield of projectile- ( $\sigma_{PLqf}$ ) and target-like ( $\sigma_{TLqf}$ ) products together with asymmetric ( $\sigma_{asymqf}$ ) and symmetric ( $\sigma_{symqf}$ ) fragments of the DNS decay:

$$\sigma_{\text{qf}} = \sigma_{PLqf} + \sigma_{TLqf} + \sigma_{asymqf} + \sigma_{symqf}. \quad (1)$$

Usually the contributions  $\sigma_{PLqf}$  and  $\sigma_{TLqf}$  to quasifission are not considered at the estimation of the capture though the strong yield of these products decreases the amount of events leading to complete fusion.

The authors of Refs. [1] and [2] have concentrated their attention to the mass region  $0.25 < M_R < 0.75$  in analysis of the mass-angle distribution of the fusion-fission products. Then the fusion-fission cross sections were considered as capture cross section since the authors had assumed that there was no hindrance to the complete fusion in the  $^{36}\text{S}+^{206}\text{Pb}$  reaction. The mass region of the quasifission products, which overlaps with the one of the projectile-like and target-like products of deep-inelastic collision, is around  $M_R = 0.15$ . The authors of Refs. [1] and [2] did not study this mass region of the reaction products.

Unfortunately, often these quasifission products are considered as products of the deep-inelastic collisions and their contribution is not included in the capture cross section at the estimation of the fusion probability  $P_{\text{CN}}$  from the analysis of the experimental data.

$$P_{\text{CN}} = \frac{\sigma_{ER} + \sigma_{\text{fusion-fission}}}{\sigma_{ER} + \sigma_{\text{fusion-fission}} + \tilde{\sigma}_{\text{qf}}}, \quad (2)$$

where  $\sigma_{ER}$  and  $\sigma_{\text{fusion-fission}}$  are the evaporation residue and fusion-fission cross sections, respectively; the cross section of quasifission estimated by the assumption of experimentalists is  $\tilde{\sigma}_{\text{qf}} = \sigma_{\text{asymqf}} + \sigma_{\text{symqf}}$ . For example, the experimental data of capture cross section presented in Ref. [8] were compared with the theoretical results in Ref. [9]. The separation of the mass symmetric products of quasifission  $\sigma_{\text{symqf}}$  from the fusion-fission products is the other interesting and difficult problem of future theoretical and experimental studies [10, 11, 12].

Therefore, the experimental value of  $P_{\text{CN}}$  is larger than its theoretical value. This means that the estimated capture cross section from the analysis of experimental data

is smaller than theoretical capture cross section calculated as a sum of the full momentum transfer events. Theoretical values of the capture cross sections are calculated with the quantities characterizing the entrance channel by formula

$$\sigma_{\text{cap}}(E_{\text{c.m.}}) = \frac{\lambda^2}{4\pi} \sum_{\ell=0}^{\ell_d} (2\ell + 1) \mathcal{P}_{\text{cap}}^{(\ell)}(E_{\text{c.m.}}), \quad (3)$$

where  $\mathcal{P}_{\text{cap}}^{(\ell)}(E_{\text{c.m.}})$  is the capture probability of the projectile-nucleus by the target-nucleus in collision with energy  $E_{\text{c.m.}}$  and orbital angular momentum  $L = \hbar\ell$ ;  $\mu$  is the reduced mass of colliding nuclei and  $\lambda = \hbar/\sqrt{2\mu E_{\text{c.m.}}}$ . All partial waves corresponding to the full momentum transfer events are included into the summation in Eq.(3). This means that Eq.(3) includes the yield of projectile- and target-like products together with fusion-fission, quasifission and evaporation residue products. The DNS formed in the collisions with the given values of  $E_{\text{c.m.}}$  and  $\ell$  evolves to complete fusion due to the transfer of all nucleons of the light fragment to the heavy one or it can decay forming binary products with charge and mass numbers in the wide range. According to our view, the projectile- and target-like products having low total kinetic energy are considered as the quasifission products. The dynamical calculation by the method presented in Section 3 allows us to find angular momentum distribution of the DNS formed in capture. In some methods of capture calculations, the variation of the maximum value of the orbital angular momentum  $\ell_d$  or another way is used to reach an agreement with the experimental values of the capture cross section which is found by ignoring the yield of the capture prod-

ucts which have close values to the initial mass and charge numbers of colliding nuclei [13].

### 3 Theoretical model

The dynamics of complete fusion in heavy ion collisions at low energies is determined by the orbital angular momentum, the charge and mass numbers, shape, orientation angles of their symmetry axis and the shell structure of the interacting nuclei. The probability of the mass and charge distributions between fragments of the DNS and the probability of its decay depend on the shell structure, the excitation energy and angular momentum of the system. Therefore, it is important to include into consideration the construction of the theoretical methods to study the role of the entrance channel in formation of the reaction products. The examples of results corresponding to the full momentum transfer events are presented in panels (b),(c) and (d) of Fig. 1.

#### 3.1 Calculation of capture cross section

Two conditions must be satisfied for the capture: 1) the initial energy  $E_{c.m.}$  of a projectile in the center-of-mass system should be enough to reach the potential well of the nucleus-nucleus interaction (Coulomb barrier + rotational energy of the entrance channel) by overcoming or tunneling through the barrier along relative distance in the entrance channel; 2) at the same time the value of the relative kinetic energy above the entrance channel barrier should in correspondence with the size of the potential

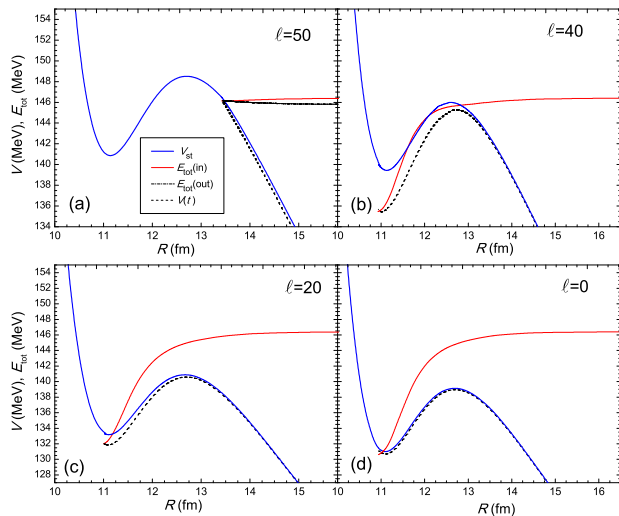


**Fig. 1.** (Color online) Deep inelastic collision (a) and capture (b),(c),(d) trajectories at collision energy  $E_{c.m.} = 146.41$  MeV for the  $^{36}\text{S} + ^{206}\text{Pb}$  reaction. The thick solid lines are the interaction potential  $V(t)$ ; thin solid and dot-dashed lines are the total energy  $E_{tot}$  of the relative motion for the incoming and outgoing trajectories (only for the case of  $L = 50\hbar$ ), respectively; the dashed lines are the time dependent interaction potential  $V(t)$  calculated taking into account damping angular momentum and nucleon exchange between nuclei [14]. The total energy  $E_{tot}$  decreases due to dissipation by the radial friction coefficient and the dynamical interaction potential  $V(t)$  presented by the dotted line while the nucleus-nucleus potential including the DNS rotational energy calculated with the undamped values of  $L$  is shown by the thick solid line.

well: in case of the collision of the massive nuclei the size of the potential is small and, if the initial collision energy is very large relative to the the entrance channel barrier, the dissipation of the kinetic energy may be not enough to make its value lower than barrier of potential well, *i.e.* to cause trapping into potential well. As a result, the cap-

ture does not occur and the deep-inelastic collision takes place (as in Fig. 2b of Ref. [14] or Fig. 1 of Ref. [15]). If there is no potential well, the deep-inelastic collision takes place only. In this work the possibility of capture by tunnelling through the Coulomb barrier, at the collision energies ( $E_{c.m.}$ ) lower than the barrier, is taken into account. In this case, at the same values of the angular momentum both capture and deep-inelastic collision can occur. Fig. 1 shows the dependence of the total energy ( $V(t) + E_{kin}$ ) of the radial motion  $E_{tot}$  and nucleus-nucleus potential on the distance  $R$  between centers of nuclei for the  $^{36}\text{S}+^{206}\text{Pb}$  reaction at the collision energy  $E_{c.m.} = 146.41$  MeV. We should note that the capture probability is calculated for all values of  $\ell$  including the case presented in Fig. 1. The capture probability by tunneling in the case showed in Fig. 1(a) is discussed later in Fig. 2. The nucleus-nucleus potential  $V(\ell, \{\alpha_i\}; R)$  consists of three parts as

$$V(\ell, \alpha_1, \alpha_2; R) = V_{\text{Coul}}(\alpha_1, \alpha_2; R) + V_{\text{nucl}}(\alpha_1, \alpha_2; R) + V_{\text{rot}}(\ell, \alpha_1, \alpha_2; R), \quad (4)$$

where  $V_{\text{Coul}}$ ,  $V_{\text{nucl}}$  and  $V_{\text{rot}}$  are the Coulomb, nuclear and rotational potentials, respectively. In the case of collision of nuclei with the deformed shape in their ground states, the dependence of the nucleus-nucleus potential on orientation angle of their axial symmetry axis should be taken into account. We refer to Ref. [16] and Appendix A of Ref. [14] for the detailed expressions of these potentials in terms of the orientation angles of the symmetry axis of the colliding nuclei.

The colliding nuclei in the  $^{34}\text{S}+^{208}\text{Pb}$  and  $^{36}\text{S}+^{206}\text{Pb}$  reactions are spherical in their ground states, therefore, possibility of the population of vibrational states at their excitation is considered. As the amplitudes of the surface vibration we use deformation parameters of first excited  $2^+$  and  $3^-$  states of the colliding nuclei. The values of the deformation parameters of first excited  $2^+$  and  $3^-$  states are presented in Table 1 which are taken from Ref(s). [17] ( $\beta_2^+$ ) and [18] ( $\beta_3^-$ ).

**Table 1.** Deformation parameters  $\beta$  and mean lifetime  $\tau$  of first excited  $2^+$  and  $3^-$  states of the colliding nuclei used in the calculations in this work.

Nucleus	$^{34}\text{S}$	$^{36}\text{S}$	$^{206}\text{Pb}$	$^{208}\text{Pb}$
$\beta_2^+$ [17]	0.252	0.168	0.0322	0.055
$\tau_{2^+}$ ( $10^{-12}$ s) [17]	0.023	0.110	0.11	0.0012
$\beta_3^-$ [18]	0.330	-	0.083	0.100
$\tau_{3^-}$ ( $10^{-12}$ s) [18]	0.130	-	-	47

The surface vibrations are regarded as independent harmonic vibrations and the nuclear radius is considered to be distributed as a Gaussian distribution [19],

$$g(\beta_2, \beta_3; \alpha) = \exp \left[ -\frac{(\sum_{\lambda} \beta_{\lambda} Y_{\lambda 0}^*(\alpha))^2}{2\sigma_{\beta}^2} \right] (2\pi\sigma_{\beta}^2)^{-1/2}, \quad (5)$$

where  $\alpha$  is the direction of the spherical nucleus. For simplicity, we use  $\alpha = 0$ :

$$\sigma_{\beta}^2 = R_0^2 \sum_{\lambda} \frac{2\lambda + 1}{4\pi} \frac{\hbar}{2D_{\lambda}\omega_{\lambda}} = \frac{R_0^2}{4\pi} \sum_{\lambda} \beta_{\lambda}^2, \quad (6)$$

where  $\omega_{\lambda}$  is the frequency and  $D_{\lambda}$  is the mass parameter of a collective mode.

The first step at the estimation of the capture cross section is the calculation of the partial capture cross sections for the seven values for each deformation parameters  $\beta_2$  and  $\beta_3$  in the corresponding ranges  $-\beta_2^+ < \beta_2 < \beta_2^+$  and  $-\beta_3^- < \beta_3 < \beta_3^-$  for the vibrational nuclei, *i.e.* the differences between intermediate values of the deformation parameters used in calculations are  $\Delta\beta_2^+ = \beta_2^+/3$  and  $\Delta\beta_2^- = \beta_2^-/3$ , respectively. This procedure is acceptable since the mean lifetime  $\tau$  of first excited  $2^+$  and  $3^-$  states (see Table 1) are much larger than interaction time of colliding nuclei at capture and complete fusion times which do not precede  $10^{-19}$  s. Therefore, deformation parameters  $\beta_2$  and  $\beta_3$  can be considered as the frozen values during the capture process.

The partial capture cross-section  $\sigma_{cap}^{(\ell)}(E_{c.m.}, \{\beta_i\})$  is determined by calculation of the capture probability  $\mathcal{P}_{cap}^{(\ell)}(E_{c.m.}, \{\beta_i\})$  of trapping the curve presenting the dependence of total kinetic energy on the time dependent internuclear distance into the potential well of the nucleus-nucleus interaction:

$$\sigma_{cap}^{(\ell)}(E_{c.m.}, \{\beta_i\}) = \frac{\lambda^2}{4\pi}(2\ell + 1)\mathcal{P}_{cap}^{(\ell)}(E_{c.m.}, \{\beta_i\}). \quad (7)$$

Here  $\lambda$  is the de Broglie wavelength of the entrance channel. The capture probability  $\mathcal{P}_{cap}^{(\ell)}(E_{c.m.}, \{\beta_i\})$ , which is calculated by classical equation of motion, is equal to 1 or 0 for given beam energy and orbital angular momentum. In dependence on the beam energy,  $E_{c.m.}$ , there is a  $\ell$ -window ( $\ell_m < \ell < \ell_d$ ) for capture as a function of orbital

angular momentum:

$$\mathcal{P}_{cap}^{(\ell)}(E_{c.m.}, \{\beta_i\}) = \begin{cases} 1, & \text{if } \ell_m < \ell < \ell_d \text{ and} \\ & E_{c.m.} > V_B, \\ 0, & \text{if } \ell < \ell_m \text{ or } \ell > \ell_d \text{ and} \\ & E_{c.m.} > V_B, \\ \mathcal{P}_{WKB}^{(\ell)}, & \text{for all } \ell \text{ if } E_{c.m.} \leq V_B, \end{cases} \quad (8)$$

where  $\ell_m$  and  $\ell_d$  are the minimum and maximum values of the orbital angular momentum  $\ell$  leading to capture at the given collision energy;  $V_B$  is the barrier of the nucleus-nucleus potential in the entrance channel;  $\mathcal{P}_{WKB}^{(\ell)}$  is probability of the barrier penetrability which is calculated by the formula is derived from the WKB approximation (see Eq. 20). The absence of capture at  $\ell < \ell_m$  means that the total energy curve as a function of  $E_{c.m.}$  is not trapped into potential well: dissipation of the initial kinetic energy is not enough to be trapped due to the restricted value of the radial friction coefficient. The number of partial waves giving a contribution to the capture is calculated by the solution of Eq(s) (9)-(13) for the radial and orbital motions simultaneously.

The collision trajectory, rotational angle, angular velocity and the moment of inertia of the DNS formed after capture for a given beam energy  $E_{c.m.}$  and orbital angular momentum  $L_0$  are found by solving the following equations of motion [14,20]:

$$\mu(R)\frac{d\dot{R}}{dt} + \gamma_R(R)\dot{R}(t) = F(R), \quad (9)$$

$$F(R) = -\frac{\partial V(R)}{\partial R} - \dot{R}^2 \frac{\partial \mu(R)}{\partial R}, \quad (10)$$

$$\frac{dL}{dt} = \gamma_\theta(R)R(t) \left( \dot{\theta}R(t) - \dot{\theta}_1 R_{1\text{eff}} - \dot{\theta}_2 R_{2\text{eff}} \right), \quad (11)$$

$$\frac{dL_1}{dt} = \gamma_\theta(R) \left[ R_{1\text{eff}} \left( \dot{\theta}R(t) - \dot{\theta}_1 R_{1\text{eff}} - \dot{\theta}_2 R_{2\text{eff}} \right) \right]$$

$$- 2a(R_{1\text{eff}}\dot{\theta}_1 - R_{2\text{eff}}\dot{\theta}_2) \Big], \quad (12)$$

$$\frac{dL_2}{dt} = \gamma_\theta(R) \left[ R_{1\text{eff}} \left( \dot{\theta}R(t) - \dot{\theta}_1 R_{1\text{eff}} - \dot{\theta}_2 R_{2\text{eff}} \right) + 2a(R_{1\text{eff}}\dot{\theta}_1 - R_{2\text{eff}}\dot{\theta}_2) \right], \quad (13)$$

$$L_0 = L(\dot{\theta}) + L_1(\dot{\theta}_1) + L_2(\dot{\theta}_2), \quad (14)$$

$$L(\dot{\theta}) = J_{\text{DNS}}(R)\dot{\theta}; \quad (15)$$

$$L_1(\dot{\theta}_1) = J_1\dot{\theta}_1; \quad (16)$$

$$L_2(\dot{\theta}_2) = J_2\dot{\theta}_2, \quad (17)$$

$$E_{\text{rot}} = \frac{J_R(R)\dot{\theta}^2}{2} + \frac{J_1\dot{\theta}_1^2}{2} + \frac{J_2\dot{\theta}_2^2}{2}, \quad (18)$$

where  $J_{\text{DNS}}$  is the DNS moment of inertia and it is calculated by the rigid-body approximation as

$$J_{\text{DNS}}(\beta_{i_1}, \beta_{i_2}; R) = \mu(R) R^2(\beta_{i_1}, \beta_{i_2}) + J_1 + J_2, \quad (19)$$

where  $R(\beta_{i_1}, \beta_{i_2})$  is the distance between the centers of nuclei at their given vibrational states  $i_1$  and  $i_2$  of colliding nuclei;  $J_R$  and  $\dot{\theta}$ ,  $J_1$  and  $\dot{\theta}_1$ ,  $J_2$  and  $\dot{\theta}_2$  are the moments of inertia and angular velocities of the DNS and its fragments, respectively. We also defined  $R_{1\text{eff}} = R_1 + a$  and  $R_{2,\text{eff}} = R_2 + a$ , where  $R_1$  and  $R_2$  are the radius of the interacting nuclei with  $a = 0.54$  fm [14]. Here,  $L_0$  and  $E_{\text{rot}}$  are determined by the initial conditions. The initial value of the relative distance  $R$  is taken equal to 20 fm; the initial values of the orbital angular momentum  $L_0$  is given in the range  $0 \div 80\hbar$  by the step  $\Delta L = 5\hbar$  since fission barrier disappears at  $\Delta L = 60\hbar$ ; the initial velocity of the projectile is determined by the values of  $E_{\text{c.m.}}$  and  $L_0$ .

The nucleus-nucleus interaction potential, radial and tangential friction coefficients and inertia coefficients are calculated in the framework of our model [14,15,16,21].

It should be stressed that friction coefficients  $\gamma_R$  and  $\gamma_\theta$  of the relative motions are sensitive to the shape of the colliding nuclei (see Ref. [14]). For simplicity in the presentation of formulas the following labels are used in Eq(s) (9)-(18) of motions  $F(R) = F(R, \{\beta_i\})$ ,  $\gamma_R(R) = \gamma_R(R, \{\beta_i\})$ ,  $\gamma_\theta(R) = \gamma_\theta(R, \{\beta_i\})$ ,  $V(R) = V(R, \{\beta_i\})$ , where  $R(t)$  is the relative distance,  $\dot{R}(t) \equiv dR(t)/dt$  is the corresponding velocity.

In sub-barrier capture processes, the barrier penetrability formula is derived from the WKB approximation and it is calculated by:

$$\mathcal{P}_{WKB}^{(\ell)}(E_{\text{c.m.}}, \{\beta_i\}) = \exp \left[ -2 \int_{R_{\text{in}}}^{R_{\text{out}}} k(R, \ell, \{\beta_i\}) dR \right], \quad (20)$$

where

$$k(R, \ell, \{\beta_i\}) = \sqrt{\frac{2\mu}{\hbar^2} (V(R, \ell, \{\beta_i\}) - E_{\text{c.m.}})}. \quad (21)$$

$R_{\text{in}}$  and  $R_{\text{out}}$  are inner and outer turning points which were estimated by  $V(R) = E_{\text{c.m.}}$ .

The second stage is an averaging by the expression (22) to find an averaged value of the partial capture cross section over surface vibrational state:

$$\langle \sigma_{\text{cap}}^{(\ell)}(E_{\text{c.m.}}) \rangle = \int_{-\beta_{2+}}^{\beta_{2+}} \int_{-\beta_{3-}}^{\beta_{3-}} \sigma_{\text{cap}}^{(\ell)}(E_{\text{c.m.}}, \beta_2, \beta_3) \times g(\beta_2, \beta_3) d\beta_2 d\beta_3. \quad (22)$$

The deformation parameters of the vibrational states can be considered as frozen during the capture process since as it is seen from the Table 1 that the mean lifetime of the first excited states  $2^+$  and  $3^-$  is much longer than the time scale of capture and fusion processes. The time scale of the capture and fusion processes is less than  $10^{-19}$  s.

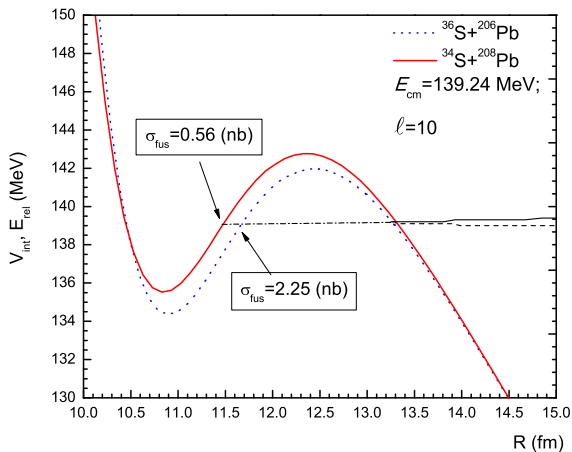


**Fig. 2.** (Color online) Deep-inelastic collision (dashed line), sub-barrier capture (dot-dashed line) and nucleus-nucleus potential for  $^{36}\text{S}+^{206}\text{Pb}$  (dotted line) and  $^{34}\text{S}+^{208}\text{Pb}$  (solid line).

Comparison of the capture probabilities calculated for the  $^{36}\text{S}+^{206}\text{Pb}$  (dotted line) and  $^{34}\text{S}+^{208}\text{Pb}$  (solid line) reactions at the collision energy  $E_{c.m.}=139.24$  MeV and  $\ell=10$  is presented in Fig. 2. The capture probability for the former reaction is about 4 times larger than the one of the latter reaction since the potential barrier calculated for the latter reaction is higher and thicker than the one for the former reaction since the projectile  $^{36}\text{S}$  has larger  $N/Z$  - ratio than  $^{34}\text{S}$ .

The role of the initial orbital angular momentum  $\ell$  in the heavy ion collisions can be seen from the Fig.3. This figure represents the dependence of the depth of the potential well and the Coulomb barrier as functions of the the orbital angular momentum for  $^{34}\text{S}+^{208}\text{Pb}$  and  $^{36}\text{S}+^{206}\text{Pb}$  reactions. It can be clearly seen that the increase of  $\ell$  can lead to reduction of the potential well.

The value of the entrance channel barrier (Coulomb barrier at  $\ell=0$ ) calculated for the  $^{34}\text{S}+^{208}\text{Pb}$  reaction is

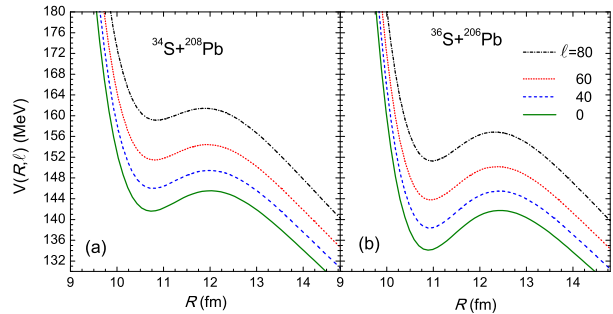


**Fig. 3.** (Color online) The influences of the rotational angular momentum on nucleus-nucleus potential; solid line for  $\ell=0$ ; dashed line for  $\ell=40$ ; dotted line for  $\ell=60$ ; dash-dotted line for  $\ell=80$  at deformation parameters presented in Table 1.

higher than the one obtained for the  $^{36}\text{S}+^{206}\text{Pb}$  reaction. The low barrier of the entrance channel is favorable to decrease the CN excitation energy since it makes lower threshold value of the beam energy leading to the CN formation.

The total capture cross section is found by summarizing over partial waves:

$$\sigma_{cap}(E_{c.m.}) = \sum_{\ell=\ell_m}^{\ell=\ell_d} \langle \sigma_{cap}^{(\ell)}(E_{c.m.}) \rangle. \quad (23)$$

It should be noted the range of orbital angular momentum values  $\ell_m < \ell < \ell_d$  contributing to capture cross section depends on the collision energy  $E_{c.m.}$ . The calculations have shown that the minimum value of angular momentum is zero ( $\ell_m=0$ ) for the  $^{34}\text{S}+^{208}\text{Pb}$  and  $^{36}\text{S}+^{206}\text{Pb}$  reactions.

### 3.2 Evolution of the DNS

The evolution of DNS to complete fusion or quasifission is determined by the landscape of potential energy surface (PES) and nucleon distribution in the single-particle

states of the interacting nuclei. The intrinsic fusion  $B_{\text{fus}}^*(Z, A)$  and  $Z = Z_P$  and the initial charge value, and quasifission  $B_{qf}(Z, A)$  barriers, as well as the excitation energy  $E_{Z,A}^*$  of DNS are found from PES. In calculation of the fusion probability, these  $B_{\text{fus}}^*(Z, A)$  and  $B_{qf}(Z, A)$  barriers are main quantities together with the DNS excitation energy  $E_{\text{DNS}}^*(Z, A)$  being functions of the mass and charge asymmetry of the DNS configuration.

The values of  $U_{dr}(Z, R_m)$  as a function of angular momentum  $\ell$  are found from the data of PES calculated by the formula and the reaction energy balance ( $Q_{gg}$ ) corresponding to the charge asymmetry configuration  $Z$  of DNS.

$$U_{dr}(Z, A, \ell, R_m) = Q_{gg} + V(Z, A, \ell, R_m) \quad (24)$$

where  $Z = Z_1$  and  $A = A_1$  are charge and mass numbers of a DNS fragment while the ones of another fragment are  $Z_2 = Z_{\text{tot}} - Z_1$  and  $A_2 = A_{\text{tot}} - A_1$ , where  $Z_{\text{tot}}$  and  $A_{\text{tot}}$  are the total charge and mass numbers of a reaction, respectively;  $Q_{gg}$  is the reaction energy balance used to determine the excitation energy of CN:  $Q_{gg} = B_1 + B_2 - B_{\text{CN}}$ . The binding energies for the initial projectile and target nuclei ( $B_1$  and  $B_2$ ) are obtained from the mass tables in Ref. [22], while the one of CN ( $B_{\text{CN}}$ ) are obtained from the mass tables [23, 24]. If there is no potential well of  $V(Z, A, R, \ell)$  at large values of angular momentum or for symmetric massive nuclei, we use  $R_m$  corresponding to the smallest value of the derivation  $\partial V(Z, A, R_m, \ell)/\partial R$  in the contact area of nuclei. The intrinsic fusion barrier,  $B_{\text{fus}}^*(Z, A, \ell)$ , is determined as the difference between the maximum value of the driving potential between  $Z = 0$

$$B_{\text{fus}}^*(Z, A, \ell) = U_{dr}^{\text{max}}(\ell) - U_{dr}(Z_P, A_P, \ell) \quad (25)$$

where  $U_{dr}^{\text{max}}(\ell) = U_{dr}(Z_{\text{max}}, A_{\text{max}}, \ell)$ .

These main quantities are found from the analysis of PES and by the use of collision energy  $E_{\text{c.m.}}$  (see [14, 25, 26]). Due to nucleon exchange between DNS nuclei their mass and charge distributions are changed as functions of time. Their evolution are estimated by solving the transport master equation with the transition coefficients calculated microscopically [27, 28]. The proton and neutron systems of nuclei have own energy scheme of the single-particle states and the single-particle schemes depend on the mass and charge numbers of nuclei. Consequently, the transition coefficients  $\Delta_K^{(-)}$  and  $\Delta_K^{(+)}$  of the transport master equation (26) being sensitive to the energy scheme and occupation numbers of the single-particle states (see Eq. (27)) of the interacting nuclei depend on the mass numbers too. The dependence of the transition coefficients  $\Delta_K^{(-)}$  and  $\Delta_K^{(+)}$  on the mass and charge numbers of nuclei leads to the correlation between proton and neutron numbers in them.

The difference between the mass and charge distributions at the given time of the DNS evolution depends on the initial  $N/Z$  - ratio in colliding nuclei since transition coefficients causing nucleon transfer are different for the isotopes with different neutron numbers of the nucleus with the same charge numbers. The difference in the mass and charge evolutions for the  $^{34}\text{S}+^{208}\text{Pb}$  and  $^{36}\text{S}+^{206}\text{Pb}$  reactions leads to the difference in fusion probabilities in these reactions. The difference in fusion cross section

immediately causes difference in the evaporation residue cross sections measured in these reactions [1].

The mass and charge distributions among the DNS fragments are calculated by solving the transport master equation:

$$\begin{aligned} \frac{\partial}{\partial t} P_K(E_K^*, \ell, t) &= \Delta_{K+1}^{(-)} P_{K+1}(E_{K+1}^*, \ell, t) \\ &+ \Delta_{K-1}^{(+)} P_{K-1}(E_{K-1}^*, \ell, t) \\ &- \left( \Delta_K^{(-)} + \Delta_K^{(+)} + \Lambda_K^{\text{qf}} \right) P_K(E_K^*, \ell, t) \end{aligned} \quad (26)$$

for  $K = Z, N$  (for proton and neutron transfers). Here  $A_1 = A = N + Z$  is the mass number of the light fragment of DNS while  $A_2 = A_{CN} - A$  and  $Z_2 = Z_{CN} - Z$  are the mass and charge numbers of the heavy fragment of DNS;  $P_K(A, E_{DNS}^*(t), \ell, t)$  is the probability of population of the configuration  $(K, K_{CN} - K)$  of the DNS at the given values of  $E_{DNS}^*(t)$ ,  $\ell$  and interaction time  $t$ . To make easy writing of the Eq(s).(26) we have used the following designations:

$$\begin{aligned} P_K(E_K^*, \ell, t) &= P_K(A, E_K^*, \ell, t), \\ P_{K\pm 1}(E_K^*, \ell, t) &= P_{K\pm 1}(A \pm 1, E_K^*, \ell, t), \\ \Delta_K^{(\mp)} &= \Delta_K^{(\mp)}(A), \\ \Delta_{K\pm 1}^{(\mp)} &= \Delta_{K\pm 1}^{(\mp)}(A \pm 1), \\ \Lambda_K^{\text{qf}} &= \Lambda_K^{\text{qf}}(A) \\ E_K^* &= E^*(K, A, \ell) \end{aligned}$$

Note these quantities and all quantities characterizing the single-particle states  $\tilde{\varepsilon}$ ,  $n_{P,T}^{(K)}$  and matrix elements  $g_{PT}^{(K)}$  in Eq.(27) depend on the mass numbers  $A$  and  $A_2 = A_{CN} - A$  of the light and heavy fragments, respectively. The transition coefficients of multinucleon transfer are calculated

as in [29]

$$\begin{aligned} \Delta_K^{(\pm)}(A) &= \frac{4}{\Delta t} \sum_{i_P, j_T} |g_{i_P j_T}^{(K)}(A)|^2 \\ &\times n_{j_T, i_P}^{(K)}(A, t) \left( 1 - n_{i_P, j_T}^{(K)}(A, t) \right) \\ &\times \frac{\sin^2[\Delta t(\tilde{\varepsilon}_{i_P}^{(K)}(A) - \tilde{\varepsilon}_{j_T}^{(K)}(A))/2\hbar]}{(\tilde{\varepsilon}_{i_P}^{(K)}(A) - \tilde{\varepsilon}_{j_T}^{(K)}(A))^2}, \end{aligned} \quad (27)$$

where the matrix elements  $g_{i_P j_T}^{(K)}(A)$  describe one-nucleon exchange between the DNS nuclei “ $P$ ” and “ $T$ ” (for the proton exchange  $K = Z$  and for the neutron exchange  $K = N$ ) and their values are calculated microscopically as in Ref.[30]. Due to dependence of the transition coefficients  $\Delta_K^{(-)}$  and  $\Delta_K^{(+)}$  on the mass and charge numbers of nuclei the neutron and proton distributions  $P_Z$  and  $P_N$  are correlated since their master equations are solved parallel way but consequently with the time step  $\Delta t$ . It is clear that the proton and neutron transfers takes place simultaneously but with the different probabilities. The letters “ $P$ ” and “ $T$ ” are used to indicate the single-particle states of nucleons in projectile-like (light) and target-like (heavy) fragments, respectively, of DNS. In the present work, we follow the scheme of Ref. [30] for estimating these values with  $\Delta t = 10^{-22}$  s  $\ll t_{\text{DNS}}$ , where  $t_{\text{DNS}}$  is the interaction time of the DNS nuclei and according to calculations it has values  $t_{\text{DNS}} > 5 \cdot 10^{-22}$  s. This way allows us to take into account non-equilibrium distribution of the excitation energy between the fragments by in calculation of the single-particle occupation numbers  $n_{i_P}^{(K)}$  and  $n_{i_T}^{(K)}$  following Ref. [31]. The excitation of the DNS is calculated by the estimation of the population of the proton and neutron hole states of one fragment under influence of the mean-field of the other fragment. This kind of evo-

lution of the single-particle occupation numbers  $n_{i_P}^{(K)}$  and  $n_{i_T}^{(K)}$  is established by solution of the Liouville quantum equation for the occupation numbers with the linearised collision term:

$$i\hbar \frac{\partial \tilde{n}_{i_P}^{(K)}(t)}{\partial t} = [H, \tilde{n}_{i_P}^{(K)}] + \frac{\tilde{n}_{i_P}^{(K)}(t) - n_{i_P}^{\text{eq}(K)}(T_Z)}{\tau_{i_P}^{(K)}}, \quad (28)$$

where  $H$  is the sum of the collective Hamiltonian  $H_{\text{rel}}$  of the relative motion of interacting nuclei of DNS, the secondary quantized Hamiltonian  $H_{\text{in}}$  of the intrinsic motion of nucleons in them and the coupling term  $V_{\text{int}}$  corresponding to the interaction between collective relative motion of nuclei and intrinsic motion of nucleons,

$$H = H_{\text{rel}} + H_{\text{in}} + V_{\text{int}}. \quad (29)$$

The last term  $V_{\text{int}}$  is responsible to excitation of the DNS fragments and it leads to evolution of the occupation numbers of nucleons. The use of the linearised collision term in Eq. (28) allows us to determine the time dependent occupation numbers evolve to the thermal equilibrium ones  $n_{i_P}^{\text{eq}(K)}(T_Z)$ ;  $\tau_{i_P}^{(K)}$  is the relaxation time of the excited single-particle state  $i_P$  of the light fragment “P” ( $i_T$  for heavy fragment “T”). The details of calculation can be find in Refs.[20,31]. The thermal equilibrium occupation numbers are calculated by the usual expression:

$$n^{\text{eq}}(T_Z) = \frac{1}{1 + \exp\left[\frac{(\tilde{\varepsilon}_{P_K} - \varepsilon_F)}{T_Z}\right]}, \quad (30)$$

where  $T_Z$  is the effective temperature of DNS with the charge asymmetry  $Z$  and its value is determined by the excitation energy  $E_{*Z}$  of DNS as the Fermi-gas temperature  $T = \sqrt{\frac{E_{*Z}}{a}}$  where  $a = 1/12 \text{ MeV}^{-1}$ .  $E_{*Z}$  is the excitation energy of DNS and it is determined by the initial

beam energy and the minimum of the potential energy as

$$E_Z^*(A, \ell) = E_{\text{c.m.}} - V(Z, A, R_m, (\ell)) + \Delta Q_{\text{gg}}(Z, A), \quad (31)$$

where  $V(Z, A, R_m, (\ell))$  is the minimum value of the potential well  $V(Z, A, R, \ell)$  at  $R_m$ ;  $\Delta Q_{\text{gg}}(Z, A) = B_1 + B_2 - B_P - B_T$  is included to take into account the change of the intrinsic energy of DNS due to nucleon transitions during its evolution along mass and charge asymmetry axes, where  $B_1$ ,  $B_2$ ,  $B_P$  and  $B_T$  are binding energies of the initial (“1” and “2”) and interacting fragments (“P” and “T”) at the given time  $t$  of interaction.

$\tilde{\varepsilon}_{P_K}$  and  $\tilde{\varepsilon}_{T_K}$  are perturbed energies of single-particle states:  $\tilde{\varepsilon}_i = \varepsilon_i + V_{ii}$ ,  $V_{ii}$  is the diagonal elements of the matrix  $V_{ii'}$  (see details in Ref(s). [27,31]). In Eq. (32),  $\Lambda_Z^{\text{qf}}$  is the Kramer’s rate for the decay probability of the DNS into two fragments with charge numbers  $Z$  and  $Z_{\text{CN}} - Z$  [32,33], which is proportional to  $\exp[-B_{\text{qf}}(Z)/(kT)]$ . The decay probability increases by decreasing the quasi-fission barrier,  $B_{\text{qf}}$ , which is taken equal to the depth of the potential well  $V(Z, A, R, \ell)$  presented in Fig(s). 1, 2 and 3.

It should be noted that the fusion probability  $P_{\text{CN}}$  is a function of the mass and charge asymmetry of the DNS nuclei and therefore, the contributions to the complete fusion of different configurations are different and their ratio depends on the time of calculation. To estimate the fusion probability in the reactions under discussion we have used the values of the master equation solutions  $P_K$  at  $t_{\text{fus}} = 6 \cdot 10^{-22}$ s starting after capture to see the effect of the non-equilibrium stage of the charge and mass distributions between nuclei of DNS. The dependence of the

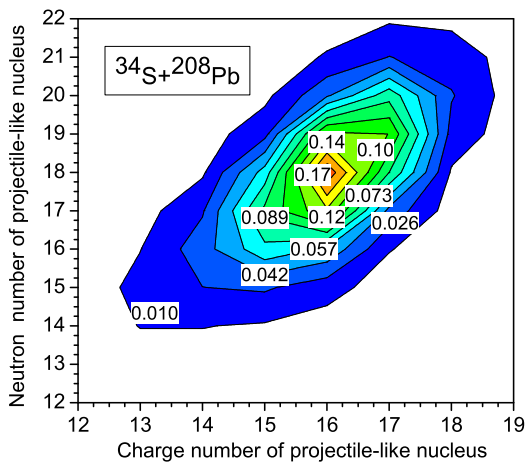


**Fig. 4.** (Color online) The dependence of the neutron distribution as a function of the charge number of the light fragment of the dinuclear system formed in the  $^{34}\text{S}+^{208}\text{Pb}$  reaction.

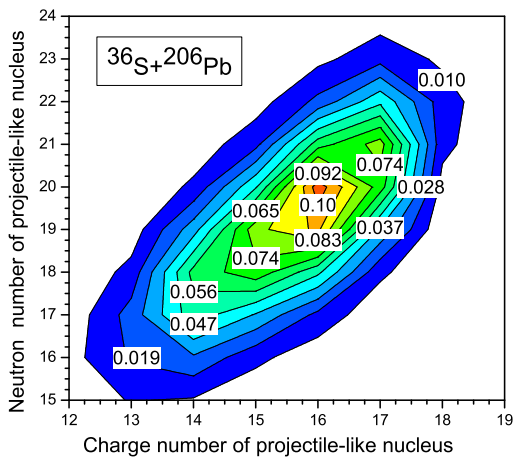


**Fig. 5.** (Color online) The same dependence of the neutron distribution as a function of the charge number of the light fragment of the dinuclear system formed in the  $^{36}\text{S}+^{206}\text{Pb}$  reaction.

neutron distribution as a function of the charge number of the light fragment of the dinuclear system formed in the  $^{34}\text{S}+^{208}\text{Pb}$  and  $^{36}\text{S}+^{206}\text{Pb}$  reactions are presented in Figs. 4 and 5, respectively.

The probability of the yield of the quasifission fragment with the mass and charge numbers,  $A$  and  $Z$ , re-

spectively, after interaction time  $t_{\text{int}}$  of DNS is estimated by

$$Y_{A,Z}(E_Z^*(A), \ell, t_{\text{int}}) = \int_0^{t_{\text{int}}} P_{A,Z}(E_Z^*(A), \ell, t) \Lambda_{A,Z}^{\text{qf}} dt, \quad (32)$$

where  $P_{A,Z}(E_{A,Z}^*, \ell, t)$  is the probability of population of the configuration  $(Z, A)$  of the DNS at the given values of the excitation energy  $E_Z^*(A)$ , angular momentum  $\ell$  and interaction time  $t$ . The interaction time  $t_{\text{int}}$  is calculated as the decay time of the DNS (details of calculation are presented in Ref. [33]). The analysis of the yield and mass distribution of quasifission products is not subject of this work. This important and interesting research is the aim of our work in future to make a conclusion about fusion mechanism of heavy nuclei.

In this work we use only mass and charge distributions  $P_{A,Z} = P_Z(A, t) \times P_N(A, t)$  which are used to find most probable values of  $N$  corresponding to the charge numbers  $Z$  of the DNS fragments. The results of calculation of neutron distribution for the given proton number for the  $^{34}\text{S}+^{208}\text{Pb}$  and  $^{36}\text{S}+^{206}\text{Pb}$  reactions are presented in Fig(s). 4 and 5, respectively. The numbers on the contours show probability of the proton and neutron distributions in the projectile-like fragments of the DNS formed at capture.

The charge number  $Z$  and corresponding mass number  $A$  are used to calculate PES which allows us to calculate the fusion probability  $P_{\text{CN}}$  as a function of the mass and charge asymmetry of the DNS nuclei. Therefore, the contributions to the complete fusion of different configu-

rations are different and their ratio depends on the time of calculation.

### 3.3 Fusion cross section

The partial fusion cross section is determined by the product of capture cross section  $\sigma_{cap}^{(\ell)}(E_{CN}^*, \{\beta_i\})$  and the fusion probability  $P_{CN}$  of DNS for the various excitation energies [16,25,26,34,35] by the use of formula:

$$\sigma_{fus}^{(\ell)}(E_{c.m.}, \{\beta_i\}) = P_{CN}(E_{c.m.}, \ell, \{\beta_i\}) \sigma_{cap}^{(\ell)}(E_{c.m.}, \{\beta_i\}), \quad (33)$$

as the sum of contributions to complete fusion from the charge symmetric configuration  $Z_{sym}$  of DNS up to configuration corresponding to the maximum value of the driving potential  $Z_{max}$ :

$$P_{CN}(E_{c.m.}, \ell, \{\beta_i\}) = \sum_{Z_{sym}}^{Z_{max}} P_Z(E_Z^*, \ell) P_{CN}^{(Z)}(E_Z^*, \ell, \{\beta_i\}), \quad (34)$$

where  $E_Z^*$  is calculated by formula (31) and the weight function  $P_Z(E_Z^*, \ell)$  is the mass and charge distributions probability  $P_Z(E_Z^*, \ell)$  in the DNS fragments is determined by solution of the transport master equation (26); the fusion probability  $P_{CN}^{(Z)}(A)$  from the charge ( $Z$ ) and mass ( $A$ ) asymmetry configuration of the DNS is calculated as the branching ratio  $P_{CN}^{(Z)}(E_Z^*, \ell; \{\alpha_i\})$  of widths related to the overflowing over the quasifission barrier  $B_{qf}(Z)$  at a given mass asymmetry, over the intrinsic barrier  $B_{fus}(Z)$  on mass asymmetry axis to complete fusion and over  $B_{sym}(Z)$  in opposite direction to the symmetric configuration of the DNS:

$$P_{CN}^{(Z)} \approx \frac{\Gamma_{fus}(Z)}{\Gamma_{qfiss}(Z) + \Gamma_{fus}(Z) + \Gamma_{sym}(Z)}. \quad (35)$$

Here, the complete fusion process is considered as the evolution of the DNS along the mass asymmetry axis overcoming  $B_{fus}(Z)$  (a saddle point between  $Z = 0$  and  $Z = Z_P = 16$ ) and ending in the region around  $Z = 0$  or  $Z = Z_{CN}$  (fig. 7). The evolution of the DNS in the direction of the symmetric configuration increases the number of events leading to quasifission of more symmetric masses. This kind of channels are taken into account by the term  $\Gamma_{sym}(Z)$ . One of the similar ways was used in Ref.[36]. The complete fusion can be presented by the formula of the width of usual fission [37]:

$$\Gamma_{fus}(Z) = \frac{\rho_{fus}(E_Z^*) T_Z}{2\pi\rho(E_Z^*)} \left( 1 - \exp\left(\frac{B_{fus}(Z) - E_Z^*}{T_Z}\right) \right), \quad (36)$$

where  $\rho_{fus}(E_Z^*) = \rho(E_Z^* - B_{fus}(Z))$ ; usually the value of the factor

$$(1 - \exp[(B_i(Z) - E_Z^*)/T_Z])$$

in (36) is approximately equal to the unit. Inserting Eq. (36) in (35), we obtain the expression (38) used in our calculations [33]:

$$P_{CN}^{(Z)}(E_Z^*) = \frac{\rho_{fus}(E_Z^*)}{\rho_{fus}(E_Z^*) + \rho_{qfiss}(E_Z^*) + \rho_{sym}(E_Z^*)}. \quad (37)$$

Putting the level density function of the Fermi system leads to formula of the calculation of fusion probability for the given values of the DNS excitation energy  $E_Z^*$  and angular momentum  $L$  from its charge asymmetry  $Z$ :

$$P_{CN}^{(Z)}(E_Z^*) = \frac{e^{-B_{fus}^{*(Z)}/T_Z}}{e^{-B_{fus}^{*(Z)}/T_Z} + e^{-B_{qfiss}^{*(Z)}/T_Z} + e^{-B_{sym}^{*(Z)}/T_Z}}. \quad (38)$$

The fusion cross section is calculated by summarizing contributions of all partial waves (angular momentum):

$$\sigma_{\text{fus}}(E_{c.m.}) = \sum_{\ell=0}^{\ell=\ell_d} \langle \sigma_{\text{fus}}^{(\ell)}(E_{c.m.}) \rangle \quad (39)$$

The averaged value of the partial fusion cross section is calculated by the same method as in the case of partial capture cross section:

$$\begin{aligned} \langle \sigma_{\text{fus}}^{(\ell)}(E_{c.m.}) \rangle &= \int_{-\beta_{2+}}^{\beta_{2+}} \int_{-\beta_{3-}}^{\beta_{3-}} \sigma_{\text{fus}}^{(\ell)}(E_{c.m.}, \beta_2, \beta_3) \\ &\times g(\beta_2, \beta_3) d\beta_2 d\beta_3. \end{aligned} \quad (40)$$

The evaporation residue cross sections after emission 2 and 3 neutrons is calculated by the use of  $\langle \sigma_{\text{fus}}^{(\ell)}(E_{c.m.}) \rangle$  to take into account the dependence of the fission barrier on the angular momentum as in Ref. [38].

## 4 Results of calculations

### 4.1 Capture of nuclei

The trajectories of the relative motion for reactions  $^{34}\text{S}+^{208}\text{Pb}$  and  $^{36}\text{S}+^{206}\text{Pb}$  at collision energies around the Coulomb barrier have been calculated by solving the equations of motion (9)-(13) for the relative distance and velocity. The bifurcation of the collision trajectories on the deep-inelastic collision and capture as a function of orbital angular momentum ( $\ell$ ) at the given collision energy  $E_{c.m.}$  is calculated by the use of the friction coefficient which is determined by the particle-hole excitation of the nucleons in nuclei and nucleon exchange between them [21]. At the sub-barrier energies the probability of capture is determined by the WKB approximation.

It is seen that the trajectory with the orbital angular momentum  $\ell = 0$  leads to capture because the relative kinetic energy is enough to overcome barrier at  $E_{c.m.} = 146.41$  MeV. The rotational energy increases by rising  $L$  and now the total energy is not enough to overcome the barrier of the interaction potential, therefore, starting from  $\ell = 50$  we observe the deep inelastic collisions only for this reaction.

As a result of the capture, we have the DNS evolved by nucleon transfer between the nuclei to reach the equilibrium mass and charge distribution which is determined by peculiarities of PES and level densities of the single-particle states of protons and neutrons in interacting nuclei. One of final states of evolution is a formation of the compound nucleus after the transferring all nucleons from the light fragment to the heavy fragment. The alternative states of the evolving DNS are its decay into two fragments in dependence on the height of  $B_{\text{qf}}$  and the DNS excitation energy.

The results obtained for the charge and mass distributions by solving master equations (26) show that initial values of the ratio of the neutron and proton numbers in colliding nuclei are important in the calculation of the fusion probability.

It is obvious from Fig. 6 that the projectile-like fragments of the DNS formed in the  $^{36}\text{S}+^{206}\text{Pb}$  reaction are more neutron rich in comparison with the ones of the  $^{34}\text{S}+^{208}\text{Pb}$  reaction. As a result the fusion probability is larger in the first reaction. Neutron numbers  $N$  corresponding to the given charge numbers presented in Fig. 6

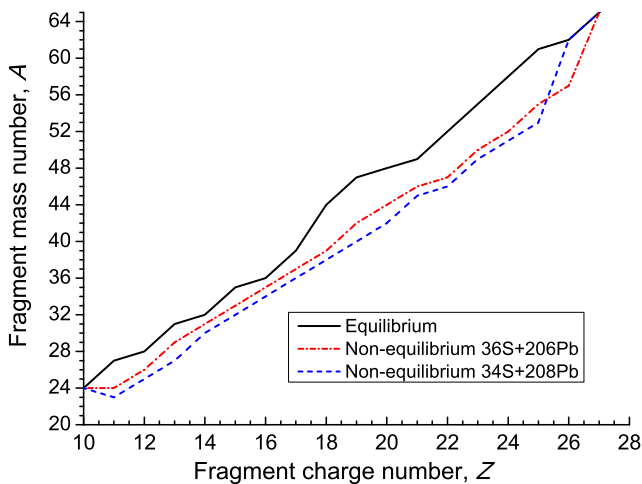


**Fig. 6.** (Color online) The mass number in the projectile nucleus as a function of its proton number calculated for  $^{36}\text{S}+^{206}\text{Pb}$  (dot-dashed line) and  $^{34}\text{S}+^{208}\text{Pb}$  (dashed line) reactions for non-equilibrium initial stage of the DNS evolution. The equilibrium distribution of neutrons between fragments corresponds to the minimum values of the PES as a function of mass numbers one of the DNS fragments (solid line).

are found from the analysis of the parallel solutions of the transport-master equations (26): the neutron number  $N$  corresponding to the maximum value of the neutron distribution function  $P_N(A, t), (K = N)$  for the given  $Z$  is used in calculation of PES. The equilibrium distribution of neutrons between fragments corresponds to the minimum values of the PES as a function of mass numbers one of the DNS fragments (solid line in Fig. 6).

So, the fusion probability of the DNS nuclei is determined by the intrinsic fusion barrier ( $B_{fus}^*$ ) and quasifission barrier ( $B_{qf}$ ) which are functions of the proton and neutron numbers (see Ref. [14]).

This result has been obtained from the neutron distributions in the light fragment of DNS as a function of its

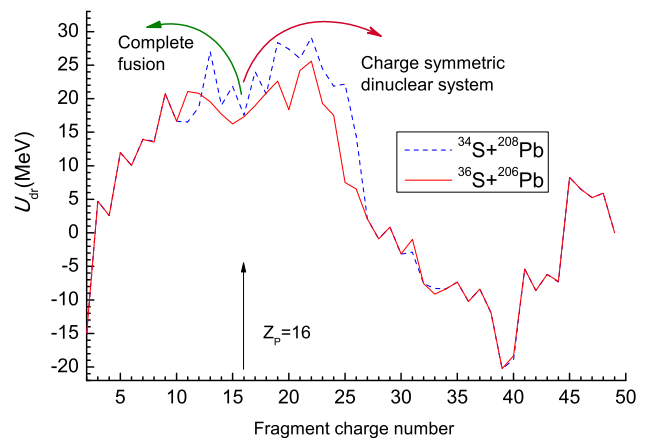


**Fig. 7.** (Color online) Driving potential calculated for the compound nuclei  $^{242}\text{Cf}$  reaction as a function of the fragment charge and mass number.

charge number at interaction time  $t_{\text{int}} = 6 \cdot 10^{-22}$  s after capture (see Figs. 4 and 5). The time preceding to capture from the beginning the dissipation of the relative energy is about  $4 \cdot 10^{-22} - 6 \cdot 10^{-22}$  s as function of the values of  $E_{\text{c.m.}}$  and  $\ell$ . It can be seen from Fig. 7 that the driving potential (blue dashed line) calculated for the  $^{34}\text{S}+^{208}\text{Pb}$  reaction increases abruptly for the fragment with charge number  $Z = 13$ . The value of the driving potential corresponding to the entrance channel  $Z = 16$  is lower than its maximum value at  $Z = 13$  in the fusion direction  $Z \rightarrow 0$ . The increase of the hindrance to complete fusion in the  $^{34}\text{S}+^{208}\text{Pb}$  reaction in comparison with the  $^{36}\text{S}+^{206}\text{Pb}$  reaction is seen from the comparison of PES in Figs. 8 and 9 which are calculated as functions of the intercentre distance between nuclei and their charge-mass asymmetry. The difference between the two PES(s) in Figs. 8 and 9 appears due to the use of the different mass numbers obtained in the solution of the Eqs. (26) by the different initial neutron numbers. As it is seen from Fig. 8 the poten-

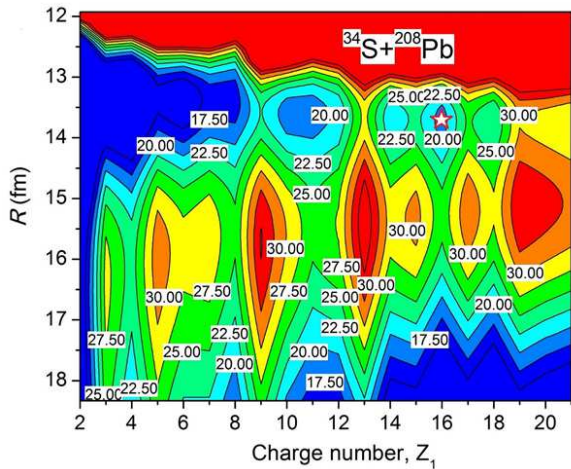


**Fig. 8.** (Color online) Contour map of the PES calculated for the  $^{34}\text{S}+^{208}\text{Pb}$  reaction with the non-equilibrium distribution of neutrons between the DNS fragments as a function of the radial distance between their mass centres and charge numbers. The point of PES corresponding to the initial charge and mass numbers is shown with a star.

tial surface has higher bump corresponding to the intrinsic fusion barrier,  $B_{fus}^*$ , in the region  $Z = 13$  and  $R = 13.5$  fm. This bump appears as the hindrance in complete fusion in the case of the  $^{34}\text{S} + ^{208}\text{Pb}$  reaction. This bump is significantly higher than the one on the potential energy surface presented in Fig. 9 for the  $^{36}\text{S} + ^{206}\text{Pb}$  reaction.

The hindrance to the DNS evolution in the direction of the symmetric charge distributions is determined by the barrier  $B_{sym}^*$  which is determined in a similar way to the case of  $B_{fus}^*$  but the maximum value of the driving potential from symmetric charge region ( $U_{dr}(Z_{max}^{sym}, A_{max}^{sym}, \ell)$ ) is used.

In Fig. 10 the capture and complete fusion cross sections are compared with the experimental data. The excitation energy of the compound nucleus  $E_{CN}^* = E_{c.m.} + Q_{gg}$

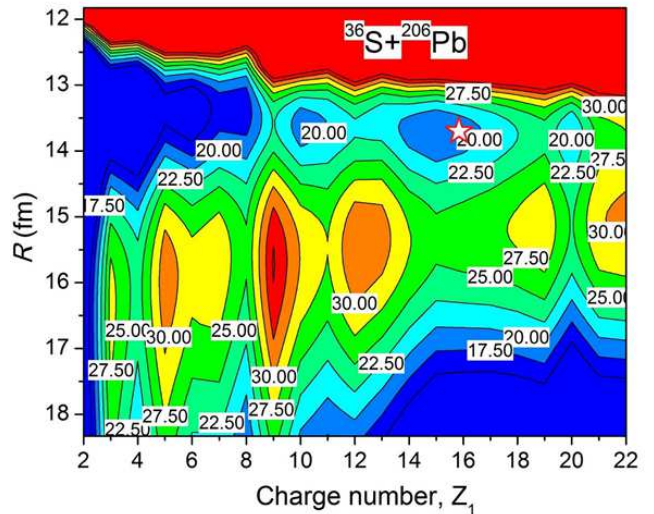


**Fig. 9.** (Color online) The same as in Fig. 8 but for the  $^{36}\text{S}+^{206}\text{Pb}$  reaction.

corresponding to the collision energy in the center of mass system  $E_{c.m.}$  has been used for the convenience of comparison of the corresponding experimental and theoretical cross sections of these reactions. It is clearly seen in Fig. 10 that the excitation fusion function of the  $^{36}\text{S}+^{206}\text{Pb}$  is much higher than the one of the  $^{34}\text{S}+^{208}\text{Pb}$  reaction in the energy region  $E_{CN}^*=24-35$  MeV, which corresponds to experimental results [1].

The lower threshold energy  $E_{CN}^{*min}$  of the fusion excitation function is determined by the height of the Coulomb barrier in the entrance channel and reaction balance energy  $Q_{gg}$ . The large negative values of  $Q_{gg}$  decrease the value of  $E_{CN}^{*min}$  [25]. The  $Q_{gg}$ -values are equal to -113.79 and -111.02 MeV for the  $^{36}\text{S}+^{206}\text{Pb}$  and  $^{34}\text{S}+^{208}\text{Pb}$  reactions, respectively. As it was discussed above as well as according to Fig. 3, the Coulomb barrier of the  $^{36}\text{S}+^{206}\text{Pb}$  reaction is lower than the one of the  $^{34}\text{S}+^{208}\text{Pb}$  reaction.

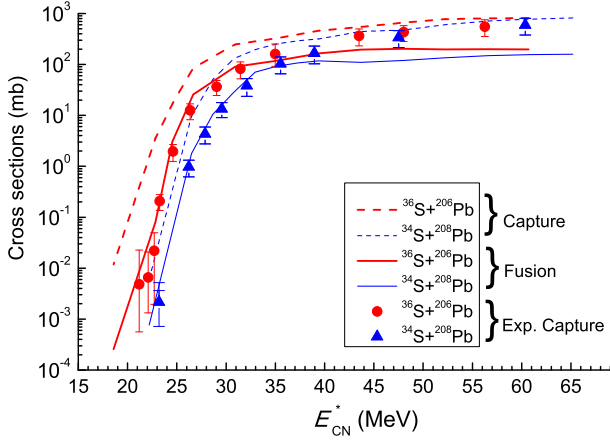


**Fig. 10.** (Color online) Capture and complete fusion cross sections calculated for  $^{36}\text{S}+^{206}\text{Pb}$  (thick and thin dashed curves) and  $^{34}\text{S}+^{208}\text{Pb}$  reactions (thick and thin solid curves) as a function of the CN excitation energy are compared with the experimental data [1].

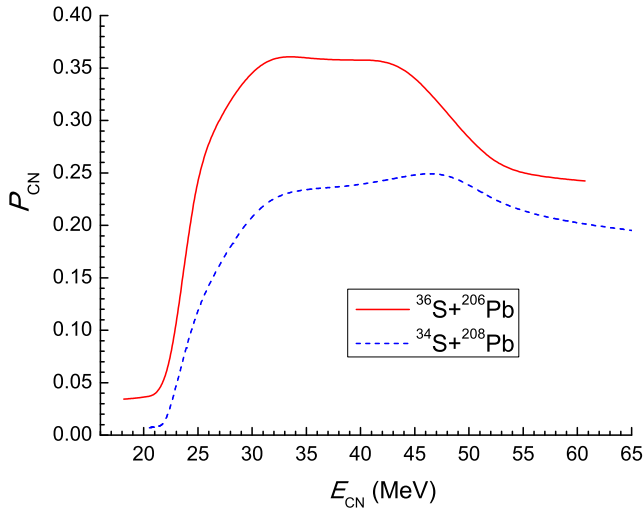


**Fig. 11.** (Color online) Fusion probability  $P_{\text{CN}}$  calculated for the  $^{36}\text{S}+^{206}\text{Pb}$  (red solid line) and  $^{34}\text{S}+^{208}\text{Pb}$  (blue dashed line) reactions.

Consequently, the threshold energy  $E_{\text{CN}}^{*min}$  for the first reaction is significantly lower than the one for the second reaction. Therefore, the condition to increase the evaporation residue cross sections has been revealed.

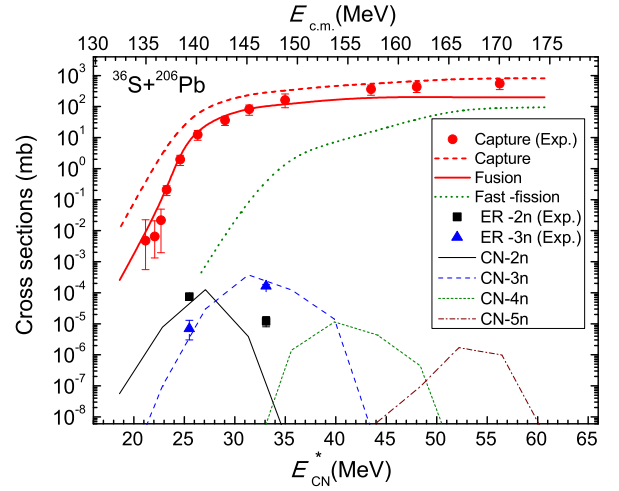


**Fig. 12.** (Color online) The theoretical values of capture (red thick dashed curve), complete fusion (solid thick curve) and ER (thin solid-2n, thin dashed-3n, thin dotted-4n and thin dot-dashed-5n channels) cross sections are compared with the experimental values of the capture (red circles) and ER (black squares-2n and red triangles-3n channels) cross sections of the  $^{36}\text{S}+^{206}\text{Pb}$  [1].

Comparison of the fusion probabilities  $P_{\text{CN}}$  calculated for the  $^{36}\text{S}+^{206}\text{Pb}$  and  $^{34}\text{S}+^{208}\text{Pb}$  reactions is presented in Fig. 11. It is seen that the complete fusion probability of the  $^{36}\text{S}+^{206}\text{Pb}$  reaction is about one and half times larger than that of the  $^{34}\text{S}+^{208}\text{Pb}$  reaction. This factor leads to the increase additionally in the difference between ER cross sections of these reactions. The large value of the capture cross section of the  $^{36}\text{S}+^{206}\text{Pb}$  reaction causes the larger value of the ER cross section of this reaction in comparison with the  $^{34}\text{S}+^{208}\text{Pb}$  reaction.

The theoretical values of capture, complete fusion and ER cross sections are compared with the experimental values of the capture and ER cross sections of the  $^{36}\text{S}+^{206}\text{Pb}$  and  $^{34}\text{S}+^{208}\text{Pb}$  reactions in Figs. 12 and 13, respectively.

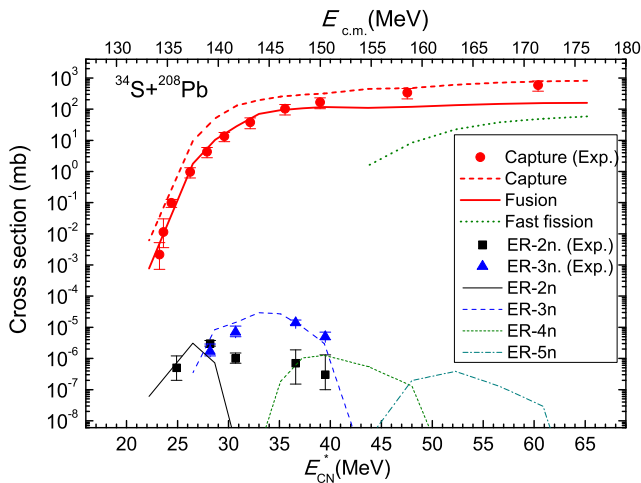


**Fig. 13.** (Color online) The same as in Fig. 12 but for the  $^{34}\text{S}+^{208}\text{Pb}$  reaction [1].

The partial fusion cross sections are used as the input data in calculations of the ER cross sections by the advanced statistical model [38]. It is seen from these figures that the theoretical results for the 3n-evaporation channel are in good agreement with the experimental data while the theoretical curve obtained for the 2n-evaporation channel is in good agreement with the data up to energies  $E_{\text{CN}}^* = 30$  MeV and 28 MeV for the  $^{36}\text{S}+^{206}\text{Pb}$  and  $^{34}\text{S}+^{208}\text{Pb}$  reactions, respectively. To reach an agreement for the 2n-evaporation channel it seems an additional assumption made in the calculation of the advanced statistical model.

## 5 Conclusion

The difference between observed cross sections of the ER of the  $^{34}\text{S}+^{208}\text{Pb}$  and  $^{36}\text{S}+^{206}\text{Pb}$  reactions formed in the 2n and 3n channels has been explained by two reasons related to the entrance channel characteristics of these reactions. The first reason is the difference in the sizes and position of the potential wells of the nucleus-nucleus in-

teraction calculated for these reactions. The presence of two extra neutrons in isotope  $^{36}\text{S}$  and projectile-like fragments makes the potential well deeper and lower for the  $^{36}\text{S}+^{206}\text{Pb}$  reaction. Therefore, the capture cross section for this reaction is larger than the one of the  $^{34}\text{S}+^{208}\text{Pb}$  reaction, *i.e.* more the number of DNS being to be transformed into compound nucleus is formed in the  $^{36}\text{S}+^{206}\text{Pb}$  reaction. The second reason is the difference in the heights of the intrinsic fusion barrier  $B_{\text{fus}}^*$  appearing on the fusion trajectory by nucleon transfer between nuclei of the DNS formed after capture. The value of  $B_{\text{fus}}^*$  calculated for the  $^{34}\text{S}+^{208}\text{Pb}$  reaction is higher than the one obtained for the  $^{36}\text{S}+^{206}\text{Pb}$  reaction. This fact is caused by the difference between the  $N/Z$ -ratios in the light fragments of the DNS formed during the capture in these reactions. The  $N/Z$ -ratio has been found by solution of the transport master equations for the proton and neutron distributions between fragments of the DNS formed at capture with the different initial neutron numbers  $N = 18$  and  $N = 20$  for the reactions with the  $^{34}\text{S}$  and  $^{36}\text{S}$ , respectively.

These reasons are related to the largest of the  $N/Z$ -ratio in the projectile-like fragments in the  $^{36}\text{S}+^{206}\text{Pb}$  reaction at the initial non-equilibrium stage of the interaction of the DNS fragments. This is seen from the comparison of the shape of the driving potentials and landscape of PES, which are calculated for these two reactions. In the DNS with the neutron-rich projectile-like fragments formed in the  $^{36}\text{S}+^{206}\text{Pb}$  reaction the intrinsic fusion barrier is lower. Due to these two consequences, the use of the neutron rich isotope  $^{36}\text{S}$  makes the ER

cross section larger in the  $^{36}\text{S}+^{206}\text{Pb}$  reaction at the de-excitation of compound nucleus in comparison with the ones of the  $^{34}\text{S}+^{208}\text{Pb}$  reaction. A larger hindrance to complete fusion in the reaction with  $^{34}\text{S}$  can be observed from the analysis of the yield of the projectile-like capture products observed in both reactions under discussion. The intense yield of the projectile-like capture products decreases the number events going to complete fusion which produces fusion-fission products and evaporation residues after emission neutrons and light charged particles.

This paper has been done in the framework of the Project F2-FA-F115 of the Committee for coordination science and technology development under the Cabinet of Ministers of Uzbekistan. The authors A.K.N. and B.M.K. thank to the committee for their financial support. A.K.N. thanks to the Russian Foundation for Basic Research for the partial support. One of the authors B.M.K. is grateful to Rare Isotope Science Project of Institute for Basic Science for the support of his staying in Daejeon. The work of K.K and Y.K is supported by the Rare Isotope Science Project of Institute for Basic Science funded by the Ministry of Science and ICT and National Research Foundation of Korea (2013M7A1A1075764).

## References

1. J. Khuyagbaatar, K. Nishio, S. Hofmann, D. Ackermann, M. Block, S. Heinz, F. P. Heßberger, K. Hirose, H. Ikezoe, B. Kindler, B. Lommel, H. Makii, S. Mitsuoka, I. Nishinaka, T. Ohtsuki, Y. Wakabayashi, and S. Yan, Phys. Rev. C **86**, 064602 (2012)
2. J. Khuyagbaatar, D. J. Hinde, I. P. Carter, M. Dasgupta, Ch. E. Dullmann, M. Evers, D. H. Luong, R. du Rietz, A. Wakhle, E. Williams, and A. Yakushev, Phys. Rev. C **91**, 054608 (2015).
3. K. Hagino *et al.*, Comput. Phys. Commun. **123**, 143 (1999).
4. W. Reisdorf, Z. Phys. A **300**, 227 (1981).
5. C. Simenel *et al.*, Phys. Lett. B **710**, 607 (2012).
6. G. Fazio, G. Giardina, G. Mandaglio, F. Hanappe, A. I. Muminov, A. K. Nasirov, W. Scheid, and L. Stuttge, Mod. Phys. Lett. A **20**, 391 (2005).
7. G. Mohanto *et al.*, Phys. Rev. C **97**, 054603 (2018).
8. G. N. Knyazheva, E. M. Kozulin, R. N. Sagaidak, A. Yu. Chizhov, M. G. Itkis, N. A. Kondratiev, V. M. Voskressensky, A. M. Stefanini, B. R. Behera, L. Corradi, E. Fioretto, A. Gadea, A. Latina, S. Szilner, M. Trotta, S. Beghini, G. Montagnoli, F. Scarlassara, F. Haas, N. Rowley, P. R. S. Gomes, and A. Szanto de Toledo, Phys. Rev. C **75**, 064602 (2007).
9. A. K. Nasirov, G. Giardina, G. Mandaglio, M. Manganaro, F. Hanappe, S. Heinz and S. Hofmann, A.I. Muminov, and C. Sacca, Phys. Rev. C **79**, 024606 (2009).
10. G. Giardina *et al.*, Jour. of Phys.: Conference Series **282**, 012006 (2011).
11. Avazbek Nasirov *et al.*, Jour. of Phys.: Conference Series **282**, 012010 (2011).
12. Meenu Thakur *et al.*, Eur. Phys. J. A **53**, 133 (2017).
13. Bing Wang, Kai Wen, Wei-Juan Zhao, En-Guang Zhao Shan-Gui Zhou, At. Data Nucl. Data Tables **114**, 282 (2017).
14. A. Nasirov, A. Fukushima, Y. Toyoshima, Y. Aritomo, A. Muminov, S. Kalandarov, and R. Utamuratov, Nucl.

- Phys. A **759**, 342 (2005).
15. G. Giardina, S. Hofmann, A. I. Muminov, A. K. Nasirov, Eur. Phys. J. A **8**, 205 (2000).
  16. G. Fazio, G. Giardina, A. Lamberto, A. I. Muminov, A. K. Nasirov, F. Hanappe, and L. Stuttgé, Eur. Phys. J. A **22**, 75 (2004).
  17. S. Raman, C. W. Nestor, JR., and P. Tikkanen, At. Data and Nucl. Data Tabl. **78**, 1 (2001).
  18. R.H. Spear, Atomic Data and Nuclear Data Tables, **42**, 55 (1989).
  19. H. Esbensen, Nuclear Physics **A352**, 141 (1981).
  20. G. G. Adamian, R. V. Jolos, A. K. Nasirov, and A. I. Muminov, Phys. Rev. C **56**, 373 (1997).
  21. A. Nasirov, B. Kayumov, Y. Oh, Nucl. Phys. A **946**, 89 (2016).
  22. G. Audi, A.H. Wapstra, Nucl. Phys. A **595**, 509 (1995).
  23. P. Möller and J.R. Nix, J. Phys. G: Nucl. Part. Phys. **20**, 1681 (1994).
  24. I. Muntian, Z. Patyk, and A. Sobczewski, Phys. At. Nuclei **66**, 1015 (2003).
  25. K.Kim, Y.Kim, A.K. Nasirov, G. Mandaglio, G. Giardina, Phys. Rev. C **91**, 064608 (2015).
  26. G. Fazio, G. Giardina, G. Mandaglio, R. Ruggeri, A. I. Muminov, A. K. Nasirov, Yu. Ts. Oganessian, A. G. Popeko, R. N. Sagaidak, A. V. Yeremin, S. Hofmann, F. Hanappe, and C. Stodel, Phys. Rev. C **72**, 064614 (2005).
  27. G. G. Adamian, A. K. Nasirov, N. V. Antonenko, and R.V. Jolos, Phys. Part. Nucl. **25**, 583 (1994)
  28. Diaz-Torres *et al*, Phys. Rev. C **64**, 014604 (2001).
  29. R. V. Jolos, A. I. Muminov, and A. K. Nasirov, Yad. Fiz. **44**, 357 (1986), [Sov. J. Nucl. Phys. **44**, 228 (1986)].
  30. G. G. Adamian, R. V. Jolos, and A. K. Nasirov, Yad. Fiz. **55**, 660 (1992), [Sov. J. Nucl. Phys. **55**, 366 (1992)].
  31. G. G. Adamian, R. V. Jolos, and A. K. Nasirov, Z. Phys. A **347**, 203 (1994).
  32. G. G. Adamian, N. V. Antonenko, and W. Scheid, Phys. Rev. C **68**, 034601 (2003).
  33. A.K. Nasirov, A.I. Muminov, R.K. Utamuratov, G. Fazio, G. Giardina, F. Hanappe, G. Mandaglio, M. Manganaro, and W. Scheid, Eur. Phys. J. A **34**, 325 (2007).
  34. G. Fazio, G. Giardina, F. Hanappe, M. Manganaro, A. I. Muminov, A. K. Nasirov, and C. Saccá, Phys. At. Nucl. **72**, 1639 (2009).
  35. N. V. Antonenko, E. A. Cherepanov, A. K. Nasirov, V. P. Permyakov, and V. V. Volkov, Phys. Lett. B **319** 425 (1993); Phys. Rev. C **51** 2635 (1995).
  36. G.G. Adamian, N.V. Antonenko, and W. Scheid, Phys. Rev. C **69**, 044601 (2004).
  37. P.J. Siemens, A.S. Jensen, Elements of Nuclei, Lecture Notes and Supplements in Physics (Addison-Wesley, Redwood City, California, 1987).
  38. G. Mandaglio, G. Giardina, A. K. Nasirov, and A. Sobczewski, Phys. Rev. C **86**, 064607 (2012).